ARTICLE

Quantitative evaluation of dissociated optic nerve fibre layer (DONFL) following idiopathic macular hole surgery

Xin Ye[1,4], Jiahao Xu[2,4], Shucheng He[1], Jun Wang[1], Jinglei Yang[1], Jiwei Tao[1], Yiqi Chen[1,3✉] and Lijun Shen[1,3✉]

OBJECTIVES: To quantitatively evaluate concentric macular dark spots (CMDS) on spectral-domain optical coherence tomography (SD-OCT) to determine the morphological characteristics of dissociated optic nerve fibre layer (DONFL) following the performance of internal limiting membrane (ILM) peeling in patients with full-thickness idiopathic macular hole (IMH) closure.

METHODS: Retrospective study on patients who underwent a vitrectomy with ILM peeling procedure. BCVA, cross-sectional OCT scans, and three-dimensional reconstructions of en face OCT scans were analysed preoperatively, at 2, 6, 12 months post-operatively. A novel image analysis technique was used to automatically measure DONFL logical properties through the radius, area, the nerve fibre layer dissociation index (NFLDI), and depth of the CMDS.

RESULTS: 53 eyes of 51 patients were included, and the mean follow-up was 11.53 ± 6.26 months. CMDS was found in 46 (86.79%) eyes within 2 months after ILM peeling and 50 (94.34%) eyes within 6 months after ILM peeling. CMDS concentrated on the temporal side of the macula in all 50 eyes (100%) at first detection. The area, NFLDI, and depth of CMDS in four quadrants developed significantly during the postoperative 6 months ($p < 0.05$), and then these changes slowed down and remained unchanged 12 months post-operatively. The morphological changes in the temporal quadrant were significantly greater than those in other quadrants at 2, 6, 12 months (all $p < 0.05$) post-operatively.

CONCLUSIONS: CMDS mostly appeared and concentrated on the temporal side of the macula in IMHs within two months after ILM peeling and progressed within 6 months and remained unchanged after 12 months.

Eye (2023) 37:1451–1457; https://doi.org/10.1038/s41433-022-02150-y

INTRODUCTION

Since Kelly and Wendel first reported successful closure of idiopathic macular holes (MH) in 1991 [1], several modifications to the surgical techniques have been proposed to improve postoperative anatomical and functional results [2]. As ILM peeling dramatically increases the anatomical closure rates in all stages of MH [3, 4], this procedure has become one of the key steps in vitrectomy [5]. ILM has been reported to act as a frame for the proliferation of cellular components such as fibroblasts, fibrocytes, and retinal pigment epithelium cells [6]. Since proliferation can lead to tangential traction, which plays an important role in MH formation [7], ILM peeling can remove the tangential traction exerted by ILM and residual cortical vitreous with a high anatomical success rate of ~80–100% [8, 9]. Despite the success, the most common complications of ILM peeling include bleeding, swelling of the arcuate retinal nerve fibre layer, dissociated optical nerve fibre layer (DONFL), macular retinal displacement, etc. In 2001, Tadayoni et al. were the first to define the arc-shaped dark area in the retina along the nerve fibre direction at the posterior pole in blue filter fundus photographs after ILM peeling procedure as DONFL [10].

Multimodal imaging methods, such as colour fundus photography, fundus photography without red light, fundus

autofluorescence, and scanning laser ophthalmoscope, have been used to evaluate DONFL in previous research. With the wide clinical application of optical coherence tomography (OCT) technology, we can observe DONFL in a more distinct way. Concentric macular dark spot (CMDS), another name of DONFL observed on en face OCT, was first proposed by Alkabes [11]. En face OCT images are coronal-view presentations generated by digitally flattening along a retinal layer boundary specifically to allow a layer-by-layer analysis of the retinal structure. This method may overcome some limitations of OCT cross-sectional images (e.g., the inability to provide a detailed evaluation of the DONFL area [12]). In Sabry's research, the CMDS was visualised on en face OCT and correlated well with the thinning areas in the GC-IPL thickness maps [13].

There also are some different views about the distribution pattern of DONFL. As Kim et al. reported, DONFL mainly occurred on the temporal side of the macula on en face OCT images [14]. However, some studies reported that DONFL with arc stripes was more frequently found in the superior quadrant in fundus photography following ILM peeling procedure [15]. These studies reveal that DONFL mainly occurs in the temporal quadrant of the macula. Nevertheless, the evaluation methods, such as counting the number of inner retinal dimples on B-scan OCT and evaluating
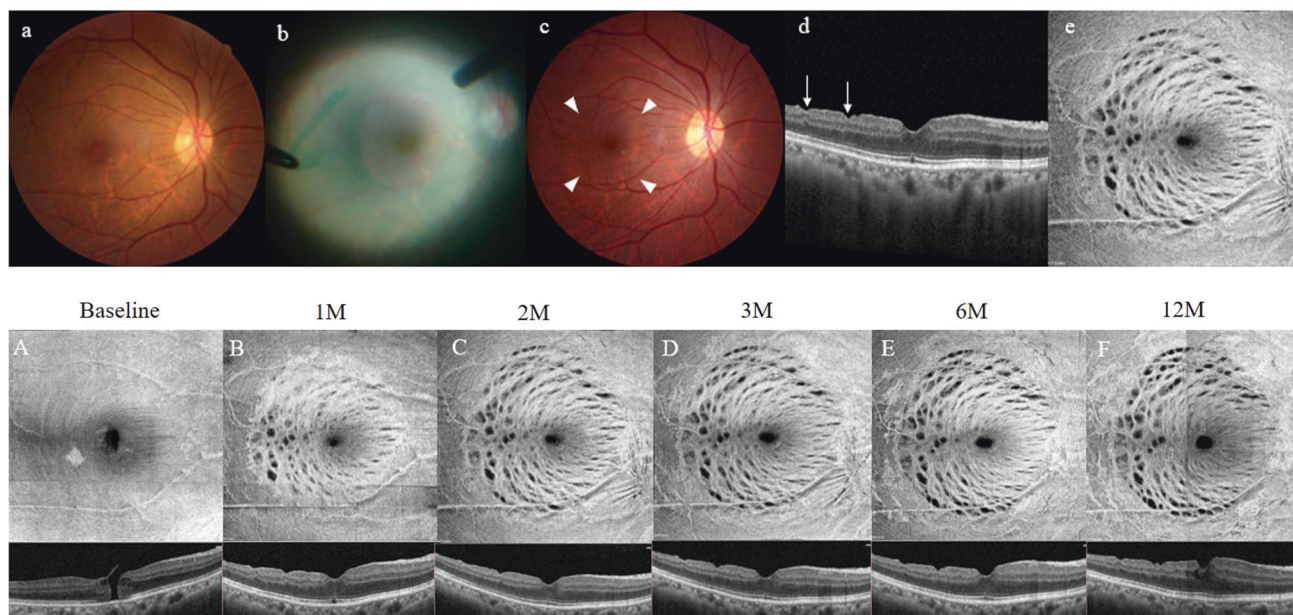
Fig. 1 Right eye of a 62-year-old woman was treated with vitrectomy and internal limiting membrane peeling for idiopathic macular hole. a Preoperative fundus photography showed a macular hole but not concentric macular dark spots (CMDS). **b** The internal limiting membrane around the macular hole was removed after indocyanine green staining. **c** Arcuate dark striae distributed along the direction of nerve fibres were observed on fundus photography at two months postoperatively. **d** Dimples of the inner retina were observed on B-scan OCT at two months postoperatively. **e** CMDS were observed on en face OCT images at 2 months postoperatively. A-F. At the 12-month postoperative follow-up point, the developmental course of CMDS on en face OCT and B-scan OCT.

the number of CMDS on en face OCT images, are still relatively simple.

An optimised automated system with a comprehensive investigation of CMDS logical properties would provide a more accurate tool for research and medical practices. Traditionally, the assessment of DONFL in MH eyes was subjective, typically including descriptors such as "mild," "moderate," or "severe." So far, none of the studies presented clear comparisons of postoperative DONFL morphology and results following ILM peeling surgery. Therefore, this study aimed to quantitatively assess the inner retinal surface following ILM peeling for FTMH over a long-term follow-up of the frequency, appearance, and development of DONFL with the use of en face and B-scan SD-OCT images. This study may enhance public awareness of DONFL following ILM peeling and refine surgical protocols in future work.

MATERIALS AND METHODS

This retrospective study reviewed the medical records of patients who underwent PPV with ILM peeling for idiopathic macular holes with a minimum follow-up of 6 months at the Affiliated Eye Hospital of Wenzhou Medical University between January 2017 and September 2020. The study was conducted in accordance with the Declaration of Helsinki and approved by the Research Ethics committee of the Affiliated Eye Hospital of Wenzhou Medical University. Informed consent to participate in the study was obtained from all of the participants.

Inclusion criteria included postoperative type 1 closed IMHs with a single surgery. Type 1 closure is defined as MHs closed with some reconstitution of the intralayer structure of the retina [16]. Exclusion criteria included other severe macular diseases, myopia <−6 dioptres, any co-morbidities including glaucoma, uveitis, and diabetic retinopathy, history of previous vitrectomy, and poor-quality OCT images during follow-up.

All surgeries were performed by a single surgeon using a 23-gauge transconjunctival vitrectomy system with an Accurus 800 CS Surgical System (Alcon Laboratories Inc., Fort Worth, TX, USA). The surgical procedure was a standard three-port PPV with triamcinolone acetonide assisted posterior vitreous detachment followed by removing as much peripheral vitreous as possible. ILM was first stained with 0.02 ml

of indocyanine green (0.025 mg/ml) and then removed in an area of 4 disc-diameters around the fovea with a pinch-and-peel technique with forceps (see Fig. 1b). After a gas–liquid exchange in the vitreous cavity, sterile air was filled. When needed, concomitant phacoemulsification with an intraocular lens was performed prior to PPV. All patients were asked to maintain a facedown position for a minimum of seven days. Ocular examination included pre- and post-operative best-corrected visual acuity (BCVA) in Snellen visual acuity chart, anterior segment, and fundus examination using slit lamp and indirect ophthalmoscopy.

OCT scanning

For each eye, a volume scan containing multiple high-density cross-sectional OCT scans was obtained using an SD-OCT (RTVue, Optovue, San Francisco, CA) with a scanning speed of 70,000 A-scans/s offering an optical axial resolution of 5 µm. A total of 400 unaveraged cross-sectional scans per acquisition, covering a 6 × 6 mm area of the macula, were taken. Only well-cantered images with signal strength index higher than 6 (out of 10) and without motion or blinking artifacts were analysed. Three-dimensional reconstructions of en face OCT images of superficial and deep retinal macular areas were obtained using the 3D Display software (RTVue, Optovue, San Francisco, CA) (see Fig. 2). OCT scans were collected to comprehensively assess preoperative as well as 3months-, 6 months-, 12 months-postoperative retinal changes three-dimensionally with four parameters: radius, area, intensity, and depth.

Manual measurement

Firstly, an estimation of CMDS distribution characteristics was generated based on the en-face OCT image. The image was divided into four different quadrants, temporal, nasal, superior, and inferior, with the fovea as the centre. The radius (r) of CMDS in each quadrant was defined as the smallest radius centred on the fovea that covers all CMDS in a single quadrant. The area of CMDS was defined as the total area of the dark spots on the en-face image. In order to estimate the intensity of CMDS, we proposed a new index, "the nerve fibre layer dissociation index" (NFLDI), which is defined as the ratio of the area of CMDS to the corresponding retinal area ($S = 1/4\pi r^2$). Manual measurement was conducted in Image J software in the following steps: (1) The en face image was imported, binarized to obtain a clear view of CMDS, and manually adjusted using Otsu's threshold tool; (2) Refer to the real distance of each pixel, the radius and total area of dark spots on the en-face image in each quadrant were measured; and (3) NFLDI was
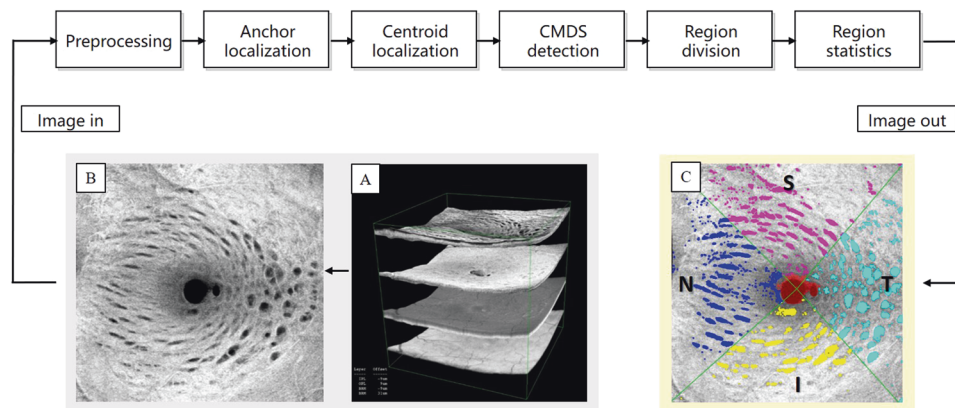
Fig. 2 Workflow of image processing and automatically measurement of CMDS. A, B En face OCT images of the superficial macular region of the retina were obtained with the RTVue XR OCT device self-contained 3D reconstruction software. **C** Automatic measurements of CMDS in the temporal, nasal, superior, and inferior quadrants, respectively.

calculated with the formula: area of CMDS divided by the total retinal area. The corresponding total retinal area calculation formula is $S = 1/4\pi r^2$.

Secondly, the depth of CMDS was measured on the cross-sectional OCT images. Dark spots on the en-face images corresponded to retinal dimples on the cross-sectional images. The two largest depth values in each quadrant were averaged and recorded.

Computer-aided auto-measurement

We developed a MATLAB-based (The MathWorks, Inc., Natick, MA, USA) programme, the nerve fibre layer dissociation index measurer (NFLDI-M), to automatically measure the area and NFLDI of CMDS after importing the two-dimensional grey-scale images. The workflow is illustrated in Fig. 2. The first step in this toolkit was to anchor four points in the surroundings of the image to crop a region that contained all the CMDS with the centre in macular. The second step was image preprocessing, including histogram equalisation and threshold segmentation, to enhance the contrast between CMDS and the background. The mask of CMDS was also obtained simultaneously. The next step was to verify the connectivity of all CMDS spots by a connected domain algorithm to compute the area in pixels and centroids of each individually connected CMDS. Since the centre of the macula was the biggest CMDS due to its depth, we developed the fourth step to define the coordinates of macula fovea by sorting all CMDS by area. The coordinates could also be chosen manually if automatic detection failed. The fifth step was to intersect two perpendicular lines (i.e., the macula fovea) to divide the image into four sub-regions: temporal, nasal, superior, and inferior. Finally, the tool would compute the area and NFLDI of each sub-region and export a report for subsequent analysis (See Fig. 2).

Man-machine comparison showed that 29 en face images (24.2%) were segmented using two toolkits (NFLDI-M and ImageJ) to determine inter-operator agreement. The inter-software reliability of the image binarization was assessed using the absolute agreement model of intra-class correlation (ICC). An ICC value over 0.81 indicated excellent agreement. ICC values less than 0.40 represented poor agreement, and it was considered moderate agreement if $0.41 < ICC < 0.80$. We also performed Bland-Altman plot analyses to visualise the mean difference between the two measurements. The Bland–Altman plots were constructed using MedCalc version 12.3 (Medcalc Software, Ostend, Belgium) software.

Statistical analyses

Statistical analyses were conducted with statistics software (IBM SPSS, version 26; IBM Corp., Armonk, NY, USA). Categorical and continuous data were expressed in percentage and mean ± standard deviation, respectively. The normality of the data distribution was confirmed using the Wilk–Shapiro test. A p value of less than 0.05 was statistically significant.

RESULTS

This study included 53 eyes of 51 patients (11 men and 42 women aged 27–83, with a mean age of 59.25 ± 9.77 years). The mean follow-up period was 11.53 ± 6.26 months, and DONFL was detected in 50 eyes (94.34%). The other demographic data are presented in Table S1.

At the first follow-up after surgery, 9 eyes (18%) had DONFL only in the temporal quadrant, and 41 eyes (82%) had DONFL in all four quadrants. Over time, DONFL was observed in all four quadrants (see Table 1 and S2). The ICCs between manual and automated measurements of CMDS area is 0.499 ($p < 0.01$), indicating a moderate agreement between the two methods. The Bland–Altman plots also confirmed a moderate agreement between two measurements for the CMDS area (Fig. S1), with a bias of 0.11 μm² and 7.9% between manual and automated measurements. The scatter plots reveal that the difference between two measurements has a positive linear correlation with the mean of the two measurements ($r = 0.77$, $p < 0.001$), indicating that manual measurement has a larger margin of error compared to automated measurement. The result was predictable based on the rough algorithm of ImageJ. To identify the CMDS area more clearly, the operator had to lower the threshold when CMDS was large and increase it when CMDS was small.

The mean radius of DONFL increased with time (1.867 ± 0.614 mm at 2 months, 2.008 ± 0.589 mm at 6 months, and 2.103 ± 0.593 mm at 12 months postoperatively). However, there were no statistically significant differences in radius between 2, 6, and 12 months postoperatively (all p values ≥ 0.05). The radius of DONFL was largest in the temporal quadrant, and there was a significant difference between the temporal radius and that of other quadrants at 2, 6, and 12 months postoperatively (all p values < 0.01, see Figs. 3 and 4). The mean area of DONFL increased with time (0.223 ± 0.249 mm² at 2 months, 0.372 ± 0.389 mm² at 6 months, and 0.385 ± 0.381 mm² at 12 months postoperatively). For each quadrant, there was a statistically significant difference between 2 and 6 months postoperatively ($p < 0.05$), while there was no statistically significant difference between 6 and 12 months postoperatively ($p ≥ 0.05$) (see Figs. 3 and 4). The area of DONFL was largest in the temporal quadrant, and there was a significant difference between the area in the temporal quadrant and the area in other quadrants at 2, 6, and 12 months postoperatively (all p values < 0.001). The mean NFLDI increased over time (7.410 ± 4.750% at 2 months, 9.889 ± 6.127% at 6 months, and 9.498 ± 6.638% at 12 months postoperatively). There was a statistically significant difference in NFLDI between 2 and 6 months postoperatively ($p < 0.05$), while no statistically significant difference was found between 6 and 12 months postoperatively ($p ≥ 0.05$). It is noteworthy that NFLDI in the temporal and inferior quadrants increased significantly from 2 months to 6 months postoperatively (temporal $p = 0.001$, inferior $p = 0.019$) (see Figs. 3 and 4). Of these, the NFLDI was largest in the temporal quadrant, and there was a significant

Table 1. Distribution parameter assessment of DONFL.

Characteristics	Quadrant of the retina				P value
	Temporal	Nasal	Superior	Inferior	
Radius (mm)					
2 months	2.296 ± 0.603	1.839 ± 0.509	1.678 ± 0.627	1.654 ± 0.497	<0.001[a]
6 months	2.404 ± 0.547	1.954 ± 0.459	1.898 ± 0.620	1.776 ± 0.539	<0.001[a]
12 months	2.580 ± 0.497	1.945 ± 0.488	1.977 ± 0.614	1.909 ± 0.515	<0.001[a]
P value	0.080[a]	0.492[a]	0.088[a]	0.099[a]	
Area (mm²)					
2 months	0.460 ± 0.368	0.153 ± 0.113	0.125 ± 0.110	0.152 ± 0.120	<0.001[a]
6 months	0.781 ± 0.535	0.221 ± 0.164	0.227 ± 0.173	0.258 ± 0.210	<0.001[a]
12 months	0.787 ± 0.489	0.243 ± 0.197	0.246 ± 0.207	0.262 ± 0.225	<0.001[a]
P value	0.001[a]	0.018[a]	0.001[a]	0.003[a]	
NFLDI (%)					
2 months	11.78 ± 5.417	6.393 ± 3.716	5.465 ± 3.780	6.005 ± 2.807	<0.001[a]
6 months	16.72 ± 6.703	8.117 ± 4.264	6.717 ± 3.345	8.005 ± 3.711	<0.001[a]
12 months	15.22 ± 6.675	7.494 ± 5.309	7.141 ± 4.089	8.140 ± 6.750	<0.001[a]
P value	0.001[a]	0.134[a]	0.130[a]	0.012[a]	
Depth (um)					
2 months	30.28 ± 8.336	21.20 ± 9.116	19.98 ± 8.368	18.78 ± 8.230	<0.001[a]
6 months	36.43 ± 6.421	28.33 ± 11.13	28.70 ± 10.77	27.75 ± 10.88	<0.001[a]
12 months	40.97 ± 11.68	30.06 ± 12.71	32.94 ± 10.68	28.97 ± 11.32	<0.001[a]
P value	<0.001[a]	<0.001[a]	<0.001[a]	<0.001[a]	

DONFL Dissociated optic nerve fibre layer, *NFLDI* Nerve fibre layer dissociation index.
[a]One-way ANOVA.

difference between the NFLDI in the temporal quadrant and other quadrants at 2, 6, and 12 months postoperatively (all p values < 0.001). The above observation and measurement results are based on the superficial retinal macular area. In addition, we observed and analysed the deep retinal layer on the en face OCT images. Of the 50 eyes that were found to have CMDS, 16 eyes (32%) had deep dark spots in the deep retinal macula area (specifically inner nuclear layer and outer plex layer) at the last follow-up (see Fig. S2).

The mean depth of CMDS increased with time (22.560 ± 9.598 µm at 2 months, 30.300 ± 10.521 µm at 6 months, and 33.234 ± 12.408 µm at 12 months postoperatively). There was a statistically significant depth difference between 2 and 6 months postoperatively ($p < 0.05$), while no statistically significant difference was found between 6 and 12 months postoperatively ($p \geq 0.05$). The depth was largest in the temporal quadrant, and there was a significant difference between the depth in the temporal quadrant and other quadrants at 2, 6, and 12 months postoperatively (all p values < 0.05) (seen in Figs. 3 and 4).

DISCUSSION
In this study, at up to 1-year postoperative follow-up, the extent and depth of DONFL involvement were greater on the temporal side of the macula, both in the early postoperative period (i.e., within 2 months) and more prolonged postoperative period (i.e., within 12 months). It is worth pointing out that DONFL is not an intended surgical outcome but an inevitable surgical result. Multiple studies confirmed that the distribution range of DONFL is restricted within the ILM exfoliation area, suggesting that the ILM exfoliation range during surgery is closely related to the occurrence and development of DONFL [11, 17]. The ILM was peeled to release traction, and the extent of dissection varied according to macular hole sizes. To reduce the impact of

differences in the extent of peeling from the surgery itself on the analysis of the distribution characteristics of DONFL, we proposed a more balanced index—NFLDI. Additionally, NFLDI was found significantly higher postoperatively in the temporal quadrant than in the other three quadrants at all follow-up time points. The reasons for this three-dimensional distribution characteristic of DONFL may be the following: (1) The clustering of retinal nerve fibres into the optic papilla causes more axons of nerve fibres on the physiological nasal side than on the temporal side, while there are more glial cells on the temporal side [18]; (2) The lack of large blood vessels in the temporal retina of the macula renders this area less capable of resisting traction and stretch [14]; (3) There were more vessels at the temporal side of the macula within the superior and inferior vascular arcades, and these vessels cause the formation of adjacent recesses; (4) The temporal nerve fibre layer is thinner, and part of retinal dimples can be traversed and more pronounced [19]; and (5) After ILM peeling, the fovea is displaced toward the optic disc, which may further enlarge the gap between the RNFL bundles temporal and the macula, making the DONFL more apparent in the temporal quadrant.

Previous studies on the development of DONFL have focused on changes in the number of inner retinal dimpling on B-scan OCT and the number of CMDS on en face OCT [20–23]. For instance, Ito et al. [24] observed that postoperatively, there were no more cases of new-onset DONFL beyond three months, and the appearance of DONFL did not change postoperatively anymore after six months. Goel et al. [25] also found that by 6 months postoperatively, all eyes no longer had newly enlarged CMDS. Our study suggests that the area, NFLDI, and depth all increase significantly in the early postoperative period, and the changes in these indicators tend to stabilise six months after surgery and as time goes.

Although the most common definition of DONFL is "defects in the nerve fibre layer (NFL)" [26], previous studies have shown that

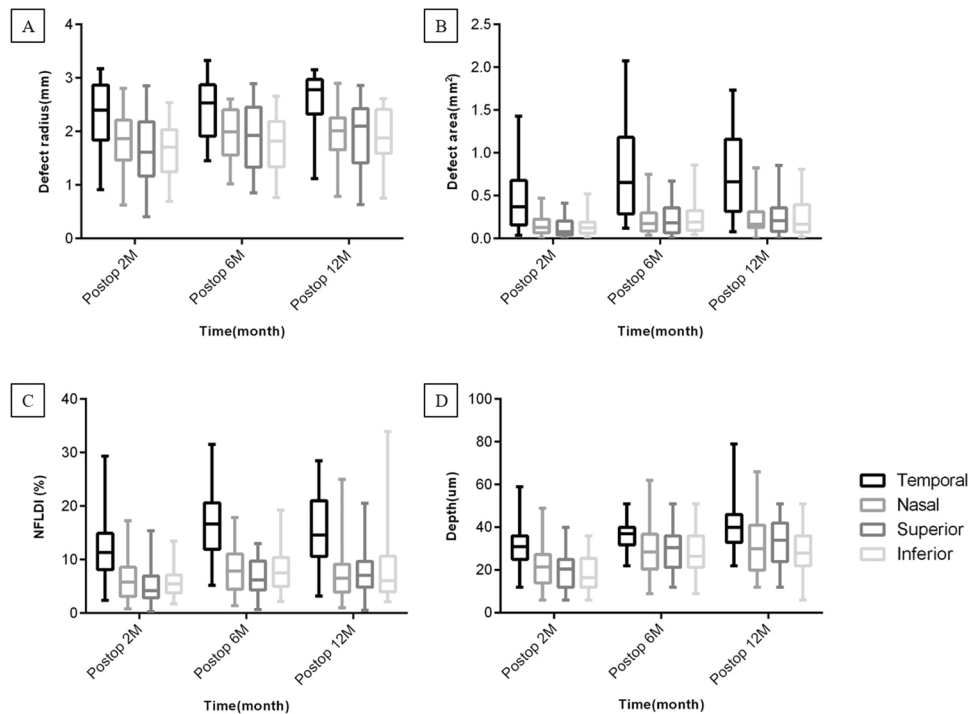**Fig. 3 Differences in the distribution of each parameter of DONFL in different quadrants were compared. A** The distribution radius of DONFL in the temporal quadrant was significantly larger than that in the other quadrants at 2, 6, and 12 months postoperatively ($p < 0.01$). **B** The DONFL area in the temporal quadrant was significantly larger than that in the other quadrants at 2, 6, and 12 months postoperatively ($p < 0.001$). **C** The nerve fibre layer dissociation index (NFLDI) in the temporal quadrant was significantly larger than that in the other quadrants at 2, 6, and 12 months postoperatively ($p < 0.001$). **D** The depth of DONFL in the temporal quadrant was significantly larger than that in the other quadrants at 2, 6, and 12 months postoperatively ($p < 0.05$). $*p < 0.05$, $**p < 0.01$, $***p < 0.001$.

DONFL is not restricted to the RNFL and that defects can reach the GCL or even the IPL. Nukada et al. [15] found that inner retinal defects extend beyond the retinal nerve fibre layer into the ganglion cell layer and inner plex layer on SD-OCT. Sabry et al. [13] divided the changes in the inner retina after ILM peeling into CMDS with intact GC-IPL and CMDS with evident localised defects in the underlying GC-IPL based on en face OCT. This study too found that the inner retinal thickness (NFL-GCL-IPL) was significantly smaller after ILM peeling, and the decrease was greater on the temporal side [13]. Considering that the NFL area did not change significantly, a reduction in GCL-IPL thickness would have occurred in deeper layers after ILM peeling. Demirel et al. [27] also reported that the GCL-IPL thickness became thinner after ILM peeling, and the GCL thinning was obvious in the inner retinal depression. Researchers have speculated that GCL thinning in the foveal area may not be caused by RGC death, but is more related to the loss or alteration of Muller cells in this region [28]. Trauma, such as injured Muller cells during ILM peeling, results in a reduction in the volume of the GCL where the Muller cell soma resides, and leads to DONFL formation [15]. In addition, dark spots were observed deeper in the retina (specifically inner nuclear layer and outer plex layer) in 32% of the eyes in our study. Muller cells reach the outer limiting membrane at the upper end and the inner limiting membrane at the lower end and are large cells that run through the full thickness of the retina. From the perspective of Muller cell injury, it seems that DONFL is not limited to RNFL. Recently, a protein involved in apoptosis (i.e., βA3/A1 crystallin) was identified [29]. This protein is not expressed in Muller cells but in retinal ganglion cells, so the inner retinal layer changes observed in the appearance of DONFL are thought to be due to ILM peeling induced by anoikis in retinal ganglion cells rather than Muller cells. Therefore, we propose that the formation of DONFL may be related to GCL-IPL defect, which may be closely related to the changes of muller cells and retinal ganglion cells. In future

studies, the pathological changes of Muller cells and retinal ganglion cells can be further verified.

The main limitations of this study are: (1) We mainly studied the three-dimensional distribution characteristics and occurrence of developmental changes in the DONFL based on OCT images, and because there were fewer patients who underwent visual function tests such as electrophysiology and microperimetry during preoperative and postoperative follow-ups, there was a lack of relevant data to explore the functional significance of OCT imaging changes; (2) Quantitative studies on DONFL were based on B-scan or en face OCT images, with the premise that a patient would maintain the same central gaze at each measurement to allow us to acquire quality OCT images of the same region. However, images from some patients could not be guaranteed to come from the same area due to influences such as patient coordination and macular hole disease severity, so there could be some measurement errors. Further studies with larger samples will be needed to reduce errors.

CONCLUSION

In conclusion, we proposed a novel image analysis technique to automatically measure DONFL logical properties in MH patients and to objectively evaluate surgical outcomes. Using only patients' OCT images, this technique can assist ophthalmologists with postoperative follow-up. In this study, CMDS were mostly found to appear and concentrate on the temporal side of the macula in the idiopathic macular hole within two months after the ILM peeling procedure. The lesion progressed within 6 months after the surgery but remained unchanged after 12 months. These findings may enhance public awareness of DONFL following ILM peeling and refine surgical protocols in future work. The ease of accessing and transferring digital images also offers the possibility of telemedicine, benefiting patients in remote areas. Moreover, this
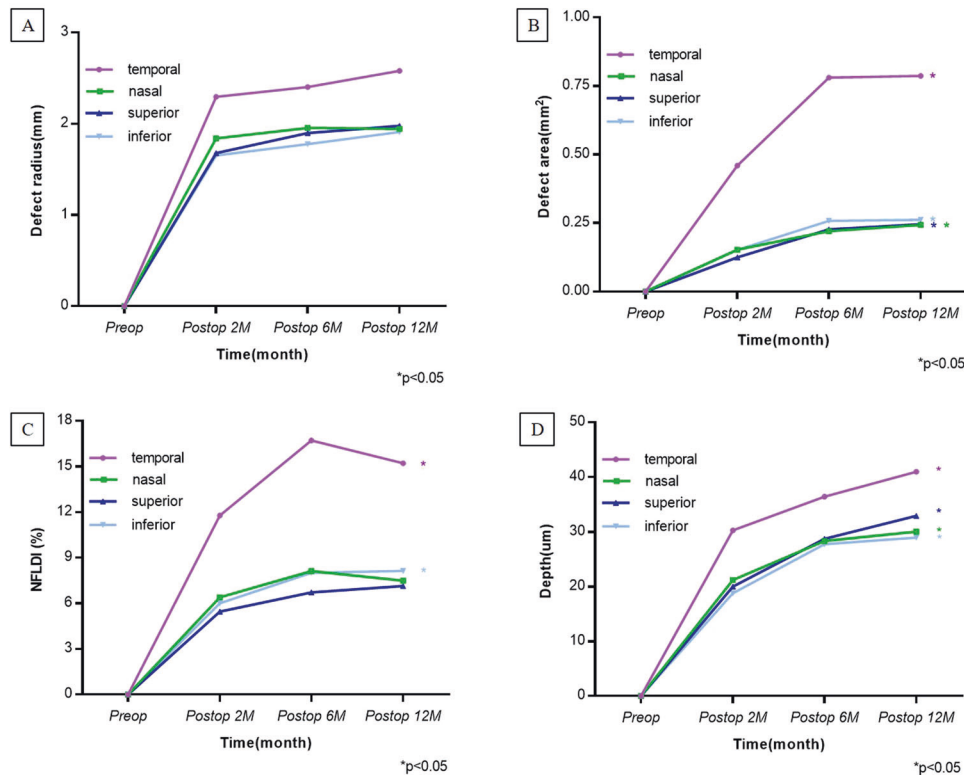
Fig. 4 Trends of changes in various parameters of CMDS during postoperative follow-ups. A The radius of distribution of CMDS in each quadrant increased during postoperative follow-ups, but none of them was statistically significant ($p > 0.05$). **B** The area of CMDS in each quadrant, except for the nasal quadrant, increased during postoperative follow-ups. The changes in CMDS area were statistically significant at 6 and 12 months after surgery, compared to the changes at 2 months ($p < 0.05$). **C** The NFLDI in the temporal and inferior quadrants increased 6 months after surgery, compared to 2 months after surgery, and the differences were statistically significant ($p < 0.05$). There were no significant differences in the nasal quadrant as well as the superior quadrant at 2, 6, and 12 months after surgery ($p > 0.05$). **D** The depth of CMDS in each quadrant increased during postoperative follow-ups, and there was statistical difference between 2 and 6 months ($p < 0.05$).

new system can have wide application potential in other retinal diseases, not limited to MH.

Summary

What was known before

- DONFL mainly occurs in the temporal quadrant of the macula and the evaluation methods are relatively simple.

What this study adds

- An optimised automated system was used to quantitatively assess the DONFL, and the frequency, appearance, and development of DONFL were clearly presented.

REFERENCES
1. Kelly NE, Wendel RT. Vitreous surgery for idiopathic macular holes. Results of a pilot study. Arch Ophthalmol. 1991;109:654–9.
2. Parravano M, Giansanti F, Eandi CM, Yap YC, Rizzo S, Virgili G. Vitrectomy for idiopathic macular hole. Cochrane Database Syst Rev. 2015;2015:Cd009080.
3. Eckardt C, Eckardt U, Groos S, Luciano L, Reale E. Removal of the internal limiting membrane in macular holes. Clinical and morphological findings. Ophthalmologe. 1997;94:545–51.
4. Brooks HL Jr. Macular hole surgery with and without internal limiting membrane peeling. Ophthalmology. 2000;107:1939–48.
5. Stec LA, Ross RD, Williams GA, Trese MT, Margherio RR, Cox MS Jr. Vitrectomy for chronic macular holes. Retina. 2004;24:341–7.
6. Semeraro F, Morescalchi F, Duse S, Gambicorti E, Russo A, Costagliola C. Current trends about inner limiting membrane peeling in surgery for epiretinal membranes. J Ophthalmol. 2015;2015:671905.
7. Steel DH, Lotery AJ. Idiopathic vitreomacular traction and macular hole: a comprehensive review of pathophysiology, diagnosis, and treatment. Eye. 2013;27:S1–21.
8. Haritoglou C, Reiniger IW, Schaumberger M, Gass CA, Priglinger SG, Kampik A. Five-year follow-up of macular hole surgery with peeling of the internal limiting membrane: update of a prospective study. Retina. 2006;26:618–22.
9. Christensen UC, Krøyer K, Sander B, Jorgensen TM, Larsen M, la Cour M. Macular morphology and visual acuity after macular hole surgery with or without internal limiting membrane peeling. Br J Ophthalmol. 2010;94:41–7.
10. Tadayoni R, Paques M, Massin P, Mouki-Benani S, Mikol J, Gaudric A. Dissociated optic nerve fiber layer appearance of the fundus after idiopathic epiretinal membrane removal. Ophthalmology. 2001;108:2279–83.
11. Alkabes M, Salinas C, Vitale L, Burés-Jelstrup A, Nucci P, Mateo C. En face optical coherence tomography of inner retinal defects after internal limiting membrane peeling for idiopathic macular hole. Investig Ophthalmol Vis Sci. 2011;52:8349–55.
12. dell'Omo R, Filippelli M, De Turris S, Govetto A, Napolitano P, dell'Omo E, et al. Multimodal imaging of lamellar macular holes. J Ophthalmol. 2021;2021:8820444.
13. Sabry D, El-Kannishy A, Kamel R, Abou Samra W. Correlation between en face optical coherence tomography defects of the inner retinal layers and ganglion cell inner plexiform layer analysis after internal limiting membrane peeling for idiopathic full-thickness macular hole. Invest Ophthalmol Vis Sci. 2016;57:OCT444–50.

14. Kim KY, Yu SY, Kim M, Kim ES, Kwak HW. Morphological change of inner retinal layer on spectral-domain optical coherence tomography following macular hole surgery. Ophthalmologica. 2013;230:18–26.

15. Nukada K, Hangai M, Ooto S, Yoshikawa M, Yoshimura N. Tomographic features of macula after successful macular hole surgery. Invest Ophthalmol Vis Sci. 2013;54:2417–28.

16. Rossi T, Bacherini D, Caporossi T, Telani S, Iannetta D, Rizzo S, et al. Macular hole closure patterns: an updated classification. Graefes Arch Clin Exp Ophthalmol. 2020;258:2629–38.

17. Mitamura Y, Ohtsuka K. Relationship of dissociated optic nerve fiber layer appearance to internal limiting membrane peeling. Ophthalmology. 2005;112:1766–70.

18. Sakimoto S, Ikuno Y, Fujimoto S, Sakaguchi H, Nishida K. Characteristics of the retinal surface after internal limiting membrane peeling in highly myopic eyes. Am J Ophthalmol. 2014;158:762–8.e1.

19. Steel DH, Dinah C, Habib M, White K. ILM peeling technique influences the degree of a dissociated optic nerve fibre layer appearance after macular hole surgery. Graefes Arch Clin Exp Ophthalmol. 2015;253:691–8.

20. Pichi F, Lembo A, Morara M, Veronese C, Alkabes M, Nucci P, et al. Early and late inner retinal changes after inner limiting membrane peeling. Int Ophthalmol. 2014;34:437–46.

21. Navajas EV, Schuck N, Govetto A, Akil H, Docherty G, Heisler M, et al. En face optical coherence tomography and optical coherence tomography angiography of inner retinal dimples after internal limiting membrane peeling for full-thickness macular holes. Retina. 2020;40:557–66.

22. Liu J, Chen Y, Wang S, Zhang X, Zhao P. Evaluating inner retinal dimples after inner limiting membrane removal using multimodal imaging of optical coherence tomography. BMC Ophthalmol. 2018;18:155.

23. Spaide RF. "Dissociated optic nerve fiber layer appearance" after internal limiting membrane removal is inner retinal dimpling. Retina. 2012;32:1719–26.

24. Ito Y, Terasaki H, Takahashi A, Yamakoshi T, Kondo M, Nakamura M. Dissociated optic nerve fiber layer appearance after internal limiting membrane peeling for idiopathic macular holes. Ophthalmology. 2005;112:1415–20.

25. Goel N, Shukla G. Long-term follow up of en face optical coherence tomography of the inner retinal surface following internal limiting membrane peeling for idiopathic macular holes. Int Ophthalmol. 2021;41:1003–10.

26. Kumar V, Dubey D, Kumawat D, Markan A, Chandra P, Chandra M, et al. Role of internal limiting membrane peeling in the prevention of epiretinal membrane formation following vitrectomy for retinal detachment: a randomised trial. Br J Ophthalmol. 2020;104:1271–6.

27. Demirel S, Abdullayev A, Yanık Ö, Batıoğlu F, Özmert E. Evaluation of ganglion cell-inner plexiform layer thickness after vitreoretinal surgery with internal limiting membrane peeling in cases with idiopathic macular hole. Turk J Ophthalmol. 2017;47:138–43.

28. Spaide RF. "Dissociated optic nerve fiber layer appearance" after internal limiting membrane removal is inner retinal dimpling. Retina. 2012;32:1719–26.

29. Ikeda T, Nakamura K, Sato T, Kida T, Oku H. Involvement of anoikis in dissociated optic nerve fiber layer appearance. Int J Mol Sci. 2021;22:1724.

COMPETING INTERESTS
The authors declare no competing interests.

CONSENT FOR PUBLICATION
Informed consent to publish was obtained from all of participants before their inclusion in the study.

ADDITIONAL INFORMATION
Supplementary information The online version contains supplementary material available at https://doi.org/10.1038/s41433-022-02150-y.

Correspondence and requests for materials should be addressed to Yiqi Chen or Lijun Shen.

Reprints and permission information is available at http://www.nature.com/reprints

Publisher's note Springer Nature remains neutral with regard to jurisdictional claims in published maps and institutional affiliations.